Geochemical Perspectives Letters

Stable W isotope evidence for redistribution of homogeneous ^{182}W anomalies in SW Greenland

F. Kurzweil, C. Münker, J.E. Hoffmann, J. Tusch, R. Schoenberg

Supplementary Information

The Supplementary Information includes:

- Geological Setting and Sample Material
- Methods, Analytical Precision and Accuracy
- The Influence of Different Mass Fractionation Laws on $\mu^{182}W$
- Figures S-1 and S-2
- Tables S-1 to S-3
- Supplementary Information References

Geological Setting and Sample Material

The Itsaq Gneiss Complex (IGC) in SW Greenland consists of up to 80 % of granitoids of the tonalite, trondhjemite-granodiorite (TTG) suite associated with complex assemblages of amphibolites, chemical and clastic sediments as well as felsic- to ultramafic units. (Moorbath *et al.*, 1973; Nutman *et al.*, 1996). Based on separate metamorphic histories it is subdivided into the Isukasia terrane (ISB and SOISB samples, Table S-1) and the Færingehavn terrane (NUK samples, Table S-1; Nutman *et al.*, 1996). Part of the Isukasia terrane is the Isua supracrustal belt (ISB), which is further divided into a 3.7 Ga old northern terrane and a 3.8 Ga old southern terrane (Nutman and Friend, 2009). Supracrustal rock assemblages and metatonalitic orthogneisses from the Northern- and Southern terrane are crosscut by the ~3.45-3.55 Ga old noritic Ameralik dykes. Juxtaposition of both terranes was dated to 3.68 Ga on a sedimentary mylonitic unit that separates both terranes (Nutman and Friend, 2009). Most rocks of the IGC were metamorphosed to amphibolite grade during at least two major metamorphic events at 3.61 Ga and 3.55 Ga (Blichert-Toft and Frei, 2001; Nutman *et al.*, 2002; Crowley, 2003). Furthermore, the IGC region experienced several phases of metasomatic alteration by fluids of locally variable composition (carbonate- and H_2O-rich; Rose *et al.*, 1996; Rosing *et al.*, 1996). The stage of deformation also varies locally including high- and low strain domains (Nutman *et al.*, 1996; Nutman and Friend, 2009).

Supracrustal rock assemblages of the IGC mainly consist of amphibolites with island arc tholeiitic geochemical affinity (herein called tholeiitic metabasalts; Polat *et al.*, 2002; Jenner *et al.*, 2009; Nutman and Friend, 2009; Hoffmann *et al.*, 2010). In the ISB typical pillow structures are locally preserved indicating low grades of deformation (Nutman and Friend, 2009). Abundant quartz globules and quartz veins contain unstrained quartz that pre-dates metamorphic fabrics. These globules and veins were interpreted to reflect chemical precipitates from circulating ocean-floor-type hydrothermal fluids (Appel *et al.*, 2001). The Northern terrane of the ISB also includes amphibolites with boninitic character that are petrogenetically unrelated to amphibolites with island arc tholeiitic affinity (Polat *et al.*, 2002; Polat and Hofmann, 2003). In contrast to the tholeiitic basalts, the boninite-like metabasalts formed by partial melting of a depleted harzburgitic mantle source, which was poor in clinopyroxene due to its progressive extraction during earlier melting events (Green, 1976; Tatsumi, 1989; van der Laan *et al.*, 1989). Boninite-like metabasalts of this study originate from the

eastern limb of the Isua Greenstone belt. Their original mineralogical composition was replaced during metamorphism by amphibole, plagioclase, chlorite, epidote, titanite and quartz (Polat *et al.*, 2002). A more detailed description of tholeiitic and boninite-like metabasalts that have been analysed for this study can be found in Polat *et al.* (2002), Hoffmann *et al.* (2010) and Tusch *et al.* (2019). In the western part of the ISB a mingling association of felsic and mafic magma was recently discovered (Boyd, 2018). The mafic unit is of tholeiitic composition. The felsic magma derived from partial melting of gabbro, which was previously altered by hydrothermal fluids (Boyd, 2018). The felsic unit shows a petrogenetic relationship to the massive felsic unit in the centre of the ISB thus not representing a late addition to the ISB (Boyd, 2018). The mingling association preserved primary magmatic structures that rather indicate the coeval eruption of felsic and mafic units, which was dated to 3808.0 ± 1.2 Ma (Boyd, 2018). Samples analysed for this study include a granular felsic rock, as well as a mafic and a leucosome enclave close to the mafic felsic contact. A more detailed description of this association can be found in Boyd (2018) and Tusch *et al.* (2019).

Metatonalitic orthogneisses and non-gneissic TTGs from the IGC represent some of the oldest fragments of continental crust (Nutman *et al.*, 1999). They formed either by melting of subducted mafic crust at high pressures (Defant and Drummond, 1990; Rapp *et al.*, 2003) or by melting of thickened island-arc crust at relatively lower pressures (Smithies, 2000; Hoffmann *et al.*, 2011; Nagel *et al.*, 2012). These felsic melts likely originated from partial melting of above mentioned tholeiites (Hoffmann *et al.*, 2011, 2014). TTGs intruded slightly older ultramafic supracrustal rock assemblages that were already deformed and metamorphosed prior to the intrusion (Nutman and Friend, 2009; Hoffmann *et al.*, 2011). Within this study non-gneissic TTGs from the ISB and a low strain area south of the ISB were also analysed. These samples consist of plagioclase, quartz, hornblende, biotite, apatite and titanite. More details can be found in Hoffmann *et al.* (2014).

The area south of the ISB also comprises ultramafic lenses that are tectonically intercalated in tonalitic gneisses and TTGs (Nutman *et al.*, 1996). In contrast to supracrustal amphibolites, these dunitic and harzburgitic enclaves might either reflect their derivative cumulates (Szilas *et al.*, 2015) or relicts of Eoarchean mantle rocks (*e.g.* van de Löcht *et al.*, 2018, 2020). Szilas *et al.* (2015) observed ultramafic units in the ISB further to the north with olivine crystals that are enclosed by serpentine. These authors interpreted the olivine to be of metamorphic origin that formed during dehydration of serpentinized rocks. The ultramafic rocks from south of the ISB analysed for this study contain olivine, orthopyroxene and amphibole with minor amounts of serpentine, biotite, chlorite and sulphides, the latter minerals being mainly linked to small veinlets (van de Löcht *et al.*, 2018, 2020). Despite the limited stability of olivine at hydrous low pressure conditions, mantle-like PGE patterns and the chemical composition of the olivines both indicate that these ultramafic units reflect mantle residues instead of cumulates (van de Löcht *et al.*, 2018). A more detailed description of our ultramafic samples can be found in Friend *et al.* (2002), van de Löcht *et al.* (2018) and Tusch *et al.* (2019).

The sediment unit that separates the Northern and the Southern terrane of the ISB mainly consists of metamorphosed and metasomatized cherts, siliciclastic turbidites, carbonates and banded iron formations. Metasediments analysed for this study are from the Garbenschiefer Formation in the western limb of the ISB having an approximate age of 3.72 Ga (Rosing, 1999; Kamber *et al.*, 1998). The mineralogical composition of these sediments comprises quartz, mica, chlorite, chalcopyrite and graphite (more details in Rosing, 1999 and Hoffmann *et al.*, 2010).

Methods, Analytical Precision and Accuracy

Short summaries of the chemical separation procedure and measurement parameters are presented in Tables S-3 and S-4. The stable W isotope composition of pure W cuts was measured using a ThermoFisher Scientific® NeptunePlus MC-ICP-MS at the University of Cologne. Details of the measurement setup parameters are provided in Kurzweil *et al.*, (2018). The iterative solution of Compston and Oversby (1969) was applied for the data reduction of individual measurement cycles assuming that the instrumental mass bias follows the exponential law. To correct for the isobaric interferences of $^{180}Hf^+$,$^{180}Ta^+$,$^{184}Os^+$, and $^{186}Os^+$ we simultaneously measured $^{177}Hf^+$,$^{181}Ta^+$ and $^{188}Os^+$ and assumed the same instrumental mass bias for these elements as for W. We present our data in the δ-notation and relative to NIST SRM 3163 in ‰:

$$\delta^{186/184}\mathrm{W} = \left(\frac{\left(\frac{^{186}W}{^{184}W}\right)_{\mathrm{Sample}}}{\left(\frac{^{186}W}{^{184}W}\right)_{\mathrm{NIST\ SRM\ 3163}}} - 1 \right) x\ 1000 \qquad \text{Eq. S-1}$$

The standard NIST SRM 3163 as well as an Alfa Aesar reference solution were repeatedly measured during measurement sequences having a long-term reproducibility in $\delta^{186/184}W$ of 0.000 ± 0.012 ‰ (n = 148) and +0.055 ± 0.016 ‰ (n = 113), respectively. Between different measurement sessions (n = 13), the average isotopic difference between Alfa Aesar and NIST SRM 3163 was very constant with $\Delta^{186/184}W$ = 0.056 ± 0.010 ‰. Additionally, the reference materials AGV-2 and BCR-2 were measured repeatedly, also including individual processing through the complete chemical separation procedure. Results for the andesitic reference material

AGV-2 (+0.007 ± 0.013 ‰; 2 s.d.; n = 6) and the basalt BCR-2 (+0.064 ± 0.006 ‰; 2 s.d.; n = 5) are consistent with previously determined compositions (Krabbe *et al.*, 2016; Kurzweil *et al.*, 2018) and confirm the previously reported 2 SD external reproducibility of ±0.018 ‰ in $\delta^{186/184}W$.

The Influence of Different Mass Fractionation Laws on $\mu^{182}W$

Mass fractionation laws relate a mass dependent isotope fractionation that is observed for one isotope ratio R_A with $R_A = N_2/N_1$ to a second isotope ratio R_B of the same element with $R_B = N_3/N_1$, where N_i is the abundance of isotope i with mass m_i. This relation can be expressed by the isotope fractionation factor $\alpha_A = \alpha_B^{\beta}$. The exponent β is a function of the masses of the isotopes and can be calculated using different mass fractionation laws (Wombacher *et al.*, 2003). For example:

Equilibrium law	$\beta = (1/m_1 - 1/m_2) / (1/m_1 - 1/m_3)$	(Young *et al.*, 2002)	Eq. S-2
Exponential (Kinetic) law	$\beta = \ln(m_1/m_2) / \ln(m_1/m_3)$	(Young *et al.*, 2002)	Eq. S-3
Power law	$\beta = (m_1 - m_2) / (m_1 - m_3)$	(Maréchal *et al.*, 1999)	Eq. S-4

The exponential and the power law represent empirical relationships to describe the instrumental mass bias during isotope measurements (Russel *et al.*, 1978; Hart and Zindler, 1989; Maréchal *et al.*, 1999). The equilibrium and the kinetic law describe theoretical considerations that follow equilibrium isotope exchange and kinetic isotope fractionation processes, respectively (Young *et al.*, 2002). In most W isotope studies mass dependent isotope fractionation that occurred during the measurement of W isotope abundances is corrected assuming the exponential mass fractionation law using a given reference value of $^{186}W/^{184}W = 0.927670$ (Völkening *et al.*, 1991). However, stable W isotope fractionation during the chemical separation of W and metasomatic alteration prior to the separation and measurement of W isotopes might be better described by another mass fractionation law such as the equilibrium law. The inappropriate application of mass fractionation laws can create apparent anomalies in single isotope abundancies (Hart and Zindle, 1989; Rizo *et al.*, 2016), an effect that will be described in more detail below.

Relative to a standard the isotope ratios R_A and R_B are expressed as δ-values with $\delta_{A\ sample} = (R_{A\ sample} / R_{A\ Std} - 1) \times 1000$ and $\delta_{B\ sample} = (R_{B\ sample} / R_{B\ Std} - 1) \times 1000$. Assuming no mass independent isotope fractionation, δ_A and δ_B are related by $\delta_B = 1000 \times [(1 + \delta_A / 1000)^{\beta} - 1)]$ (*e.g.* Farquhar *et al.*, 2002). The larger the difference in δ_A (which is calculated as difference to an unfractionated modern mantle $\delta^{186/184}W$ value of +0.085 ‰ with $\delta_A = \delta_{A\ sample} - \delta_{A\ modern\ mantle}$ Kurzweil *et al.*, 2019), the larger is the difference between δ_B that is calculated using the exponential law and δ_B that is calculated using the equilibrium law. Accordingly, R_B ratios are also slightly different, which results in relative excesses/depletions of the isotope N_3. This excess/depletion can be estimated by $\mu^{N3} = (R_B\ law_1 / R_B\ law_2 - 1) \times 10^6$. For example, for $N_1 = {}^{184}W$, $N_2 = {}^{186}W$, $N_3 = {}^{182}W$ we get $R_A = {}^{186}W/{}^{184}W$ and $R_B = {}^{182}W/{}^{184}W$. Relative to the modern upper mantle, samples from the IGC show a maximum in $\delta^{186/184}W$ of +0.164 ‰ and a minimum in $\delta^{186/184}W$ of -0.157 ‰, respectively. Using the β value of the equilibrium law (law1) and the exponential law (law2) and a $^{182}W/^{184}W$ ratio of 0.864780 (Völkening *et al.*, 1991), the $\mu^{182}W_{Equilibrium}$ is then -1.8 ppm for the maximum $\delta^{186/184}W$ value and +1.7 ppm for the minimum $\delta^{186/184}W$ value (Fig. S-2; Table S-3). Using the β value of the power law (law1) and the exponential law (law2), the $\mu^{182}W_{Power}$ is +1.8 ppm for the maximum $\delta^{186/184}W$ value and -1.7 ppm for the minimum $\delta^{186/184}W$ value (Fig. S-2; Table S-3). Thus, the application of different mass fractionation laws can theoretically only account for apparent excesses in ^{182}W that are smaller than 2 ppm (Fig. S-2; Table S-3).

Supplementary Figures

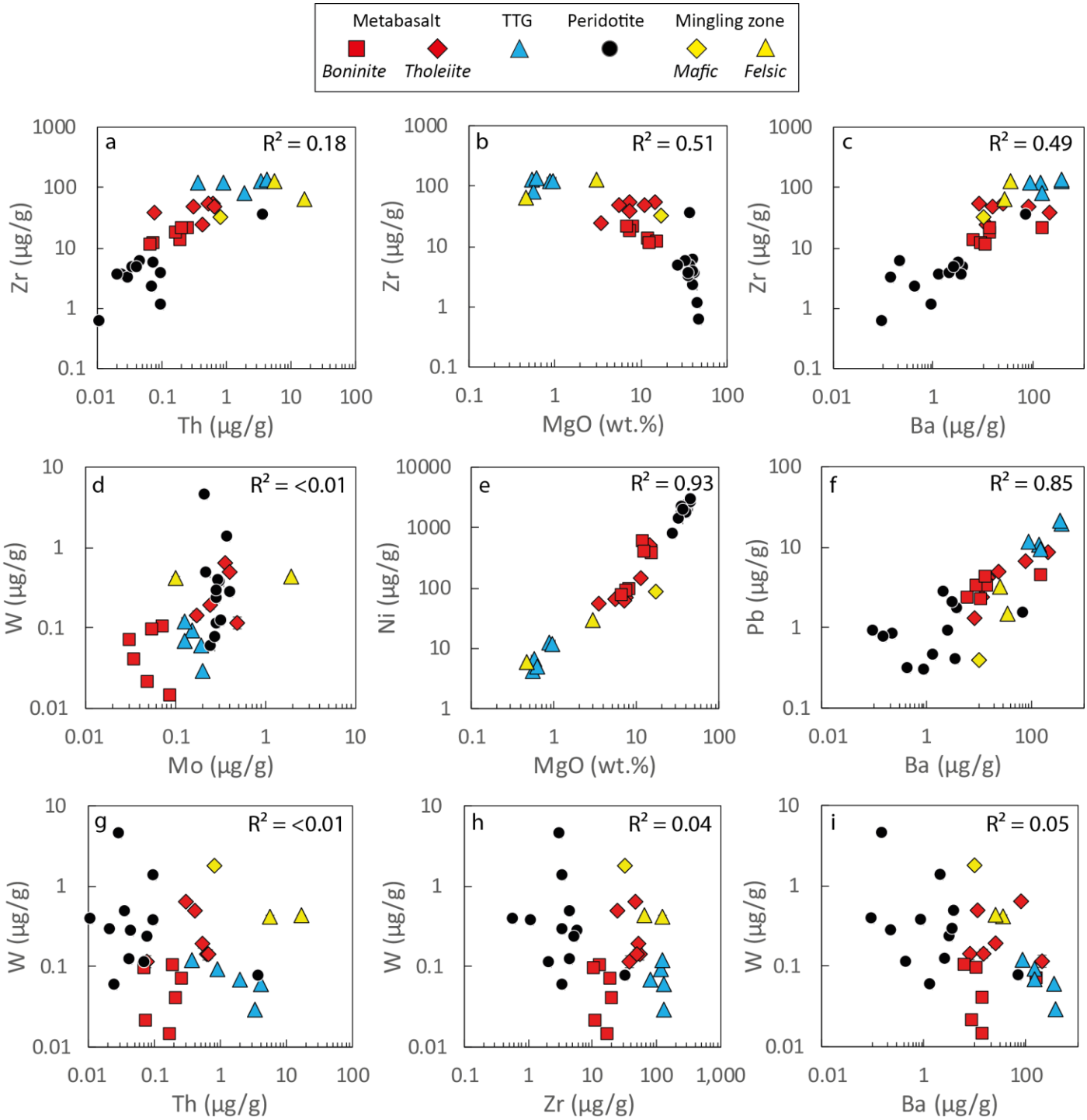

Figure S-1 **(a-f)** Trace element variation diagrams illustrating that our samples exhibit linear co-variations between various compatible and incompatible element concentrations. Most incompatible elements (Zr, Th, Nb, Ba, Pb) show expected enrichments in more differentiated rocks **(a-d, f)**, whereas compatible elements such as Mg, Ni are more depleted **(b, e)**. These differentiation trends are also preserved for some fluid mobile elements such as Ba and Pb **(c-f)**. However, the incompatible and fluid mobile element W shows no co-variation with any other parameter (**g-i**; red squares: Boninitic metabasalts, red diamonds: tholeiitic metabasalts, yellow diamonds: TTGs, black circles: mantle peridotite).

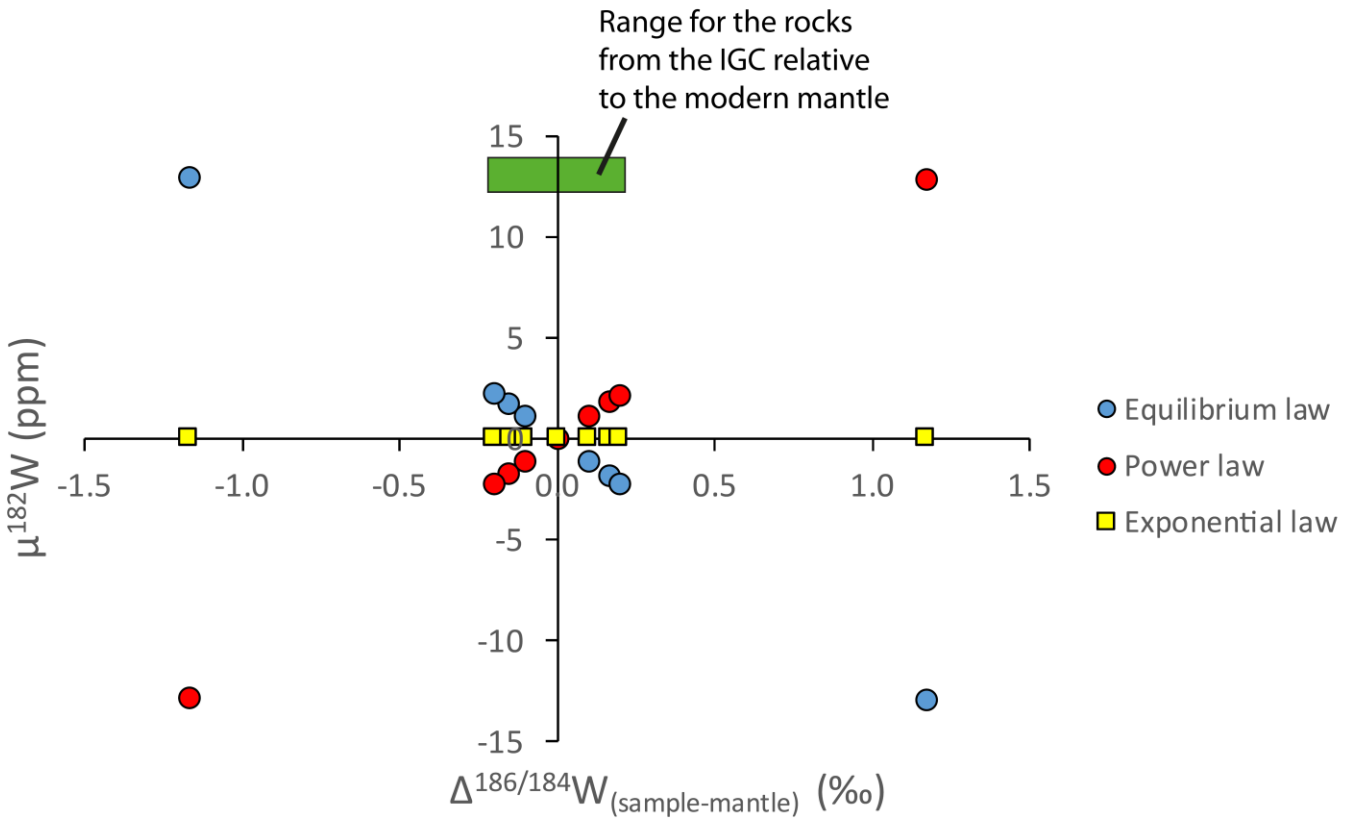

Figure S-2 In most W isotope studies mass dependent isotope fractionation that occurred during the chemical separation of W and the measurement of W isotope abundances is corrected assuming the exponential mass fractionation law. However, natural stable W isotope fractionation prior to the separation and measurement of W isotopes might be better described by another mass fractionation law. This figure shows the apparent excesses/depletions in ^{182}W that is generated by the exponential law although previous natural stable W isotope fractionation followed a different law. The larger the observed range in stable W isotope compositions relative to an unfractionated modern mantle $\delta^{186/184}W$ value of +0.085 ‰ ($\delta^{186/184}W = \delta^{186/184}W_{sample} - \delta^{186/184}W_{modern\ mantle}$), the larger is the relative apparent excess/depletion in ^{182}W ($\mu^{182}W = \{[(^{182}W/^{184}W)_{sample} / (^{182}W/^{184}W)_{SRM\ 3163}] -1\} \times 10^6$, whereby isotope ratios were previously corrected for instrumental mass bias using the exponential law and a given $^{186}W/^{184}W$ of 0.927672; Völkening *et al.*, 1991). The green shaded area indicates the range observed for rocks of the IGC in SW Greenland relative to a modern mantle $\delta^{186/184}W$ of +0.085 ‰. The excesses in $\mu^{182}W$ of around +13 ppm that are observed in rocks of the IGC (Willbold *et al.*, 2011; Rizo *et al.*, 2016; Dale *et al.*, 2017; Tusch *et al.*, 2019) represent no analytical artefacts due to the application of inappropriate mass fractionation laws.

Supplementary Tables

Data Tables S-1 to S-3 are available to download from the online version of this article at http://www.geochemicalperspectivesletters.org/article2024.

Table S-1 Tungsten concentration and stable isotope composition.

Table S-2 Available literature data of the analysed sample set (references below).

Table S-3 Calculation of apparent ^{182}W anomalies due to the application of different mass fractionation laws.

Supplementary Information References

Appel, P.W.U., Rollinson, H.R., Touret, J.L.R. (2001) Remnants of an Early Archaean (> 3.75 Ga) sea-floor, hydrothermal system in the Isua Greenstone Belt. *Precambrian Research* 112, 27–49.

Blichert-Toft, J., Frei, R. (2001) Complex Sm-Nd and Lu-Hf isotope systematics in metamorphic garnets from the Isua supracrustal belt, West Greenland. *Geochimica et Cosmochimica Acta* 65, 3177–3189.

Boyd, A.J. (2018) Geochemical Dynamics of the Isua Supracrustal Belt and the Eoarchean Earth Ph.D. Thesis. University of Copenhagen.

Compston, W., Oversby, V.M. (1969) Lead isotopic analysis using a double spike. *Journal of Geophysical Research* 74, 4338–4348.

Crowley, J.L. (2003) U–Pb geochronology of 3810–3630 Ma granitoid rocks south of the Isua greenstone belt, southern West Greenland. *Precambrian Research* 126, 235–257.

Dale, C.W., Kruijer, T.S., Burton, K.W. (2017) Highly siderophile element and 182W evidence for a partial late veneer in the source of 3.8 Ga rocks from Isua, Greenland. *Earth and Planetary Science Letters* 458, 394–404.

Defant, M.J., Drummond, M.S. (1990) Derivation of some modern arc magmas by melting of young subducted lithosphere. *Nature* 347, 662.

Farquhar, J., Wing, B.A., Mckeegan, K.D., Harris, J.W., Cartigny, P., Thiemens, M.H. (2002) Mass-independent sulfur of inclusions in diamond and sulfur recycling on early Earth. *Science* 298, 2369–2372.

Friend, C., Bennett, V., Nutman A. (2002) Abyssal peridotites> 3,800 Ma from southern West Greenland. *Contributions to Mineralogy and Petrology* 143, 71–92.

Green, D.H. (1976) Experimental testing of" equilibrium" partial melting of peridotite under water-saturated, high-pressure conditions. *The Canadian Mineralogist* 14, 255–268.

Hart, S.R., Zindler, A. (1989) Isotope fractionation laws. *International Journal of Mass Spectrometry and Ion Processes* 89, 287–301.

Hoffmann, J.E., Münker, C., Polat, A., König, S., Mezger, K., Rosing, M.T. (2010) Highly depleted Hadean mantle reservoirs in the sources of early Archean arc-like rocks, Isua supracrustal belt, southern West Greenland. *Geochimica et Cosmochimica Acta* 74, 7236–7260.

Hoffmann, J.E., Münker, C., Næraa, T., Rosing, M.T., Herwartz, D., Garbe-Schönberg, D., Svahnberg, H. (2011) Mechanisms of Archean crust formation inferred from high-precision HFSE systematics in TTGs. *Geochimica et Cosmochimica Acta* 75, 4157–4178.

Hoffmann, J.E., Nagel, T.J., Muenker, C., Næraa, T., Rosing, M.T. (2014) Constraining the process of Eoarchean TTG formation in the Itsaq Gneiss Complex, southern West Greenland. *Earth and Planetary Science Letters* 388, 374–386.

Jenner, F.E., Bennett, V.C., Nutman, A.P., Friend, C.R., Norman, M.D., Yaxley, G. (2009) Evidence for subduction at 3.8 Ga. *Chemical Geology* 261, 83–98.

Kamber, B.S., Moorbath, S. (1998) Initial Pb of the Amıtsoq gneiss revisited. *Chemical Geology* 150, 19–41.

Krabbe, N., Kruijer, T.S., Kleine, T. (2017) Tungsten stable isotope compositions of terrestrial samples and meteorites determined by double spike MC-ICPMS. *Chemical Geology* 450, 135–144.

Kurzweil, F., Münker, C., Tusch, J., Schoenberg, R. (2018) Accurate stable tungsten isotope measurements of natural samples using a 180W-183W double-spike. *Chemical Geology* 476, 407–417.

Kurzweil, F., Münker, C., Grupp, M., Braukmüller, N., Fechtner, L., Christian, M., Hohl, S.V., Schoenberg, R. (2019) The stable tungsten isotope composition of modern igneous reservoirs. *Geochimica et Cosmochimica Acta* 251, 176–191.

Maréchal, C.N., Télouk, P., Albarède, F. (1999) Precise analysis of copper and zinc isotopic compositions by plasma-source mass spectrometry. *Chemical Geology* 156, 251–273.

Moorbath, S., O'nions, R.K., Pankhurst, R.J. (1973) Early Archaean age for the Isua iron formation, West Greenland. *Nature* 245, 138.

Nagel, T.J., Hoffmann, J.E., Münker, C. (2012) Generation of Eoarchean tonalite-trondhjemite-granodiorite series from thickened mafic arc crust. *Geology* 40, 375–378.

Nutman, A.P., Allaart, J.H., Bridgwater, D., Dimroth, E., Rosing M.T. (1984) Stratigraphic and geochemical evidence for the depositional environment of the early Archaean Isua supracrustal belt, southern West Greenland. *Precambrian Research* 25, 365–396.

Nutman, A.P., Mcgregor, V.R., Friend, C.R.L., Bennett, V.C., Kinny, P.D. (1996) The Itsaq gneiss complex of southern West Greenland; the world's most extensive record of early crustal evolution (3900-3600 Ma). *Precambrian Research* 78, 1–39.

Nutman, A.P., Bennett, V.C., Friend, C.R.L., Norman, M.D. (1999) Meta-igneous (non-gneissic) tonalites and quartz-diorites from an extensive ca. 3800 Ma terrain south of the Isua supracrustal belt, southern West Greenland. *Contributions to Mineralogy and Petrology* 137, 364–388.

Nutman, A.P., Friend, C.R.L., Bennett, V.C. (2002) Evidence for 3650–3600 Ma assembly of the northern end of the Itsaq Gneiss Complex, Greenland. *Tectonics* 21.

Nutman, A.P., Friend, C.R.L. (2009) New 1. *Precambrian Research* 172, 189–211.

Polat, A., Hofmann, A.W., Rosing, M.T. (2002) Boninite-like volcanic rocks in the 3.7–3.8 Ga Isua greenstone belt, West Greenland. *Chemical Geology* 184, 231–254.

Polat, A., Hofmann, A.W. (2003) Alteration and geochemical patterns in the 3.7–3.8 Ga Isua greenstone belt, West Greenland. *Precambrian Research* 126, 197–218.

Rapp, R.P., Shimizu, N., Norman, M.D. (2003) Growth of early continental crust by partial melting of eclogite. *Nature* 425, 605.

Rizo, H., Walker, R.J., Carlson, R.W., Touboul, M., Horan, M.F., Puchtel, I.S., Boyet, M., Rosing, M.T. (2016) Early Earth differentiation investigated through 142Nd, 182W, and highly siderophile element abundances in samples from Isua, Greenland. *Geochimica et Cosmochimica Acta* 175, 319–336.

Rose, N.M., Rosing, M.T., Bridgwater, D. (1996) The origin of metacarbonate rocks in the Archaean Isua supracrustal belt, West Greenland. *American Journal of Science* 296, 1004–1044.

Rosing, M.T., Rose, N.M., Bridgwater, D., Thomsen, H.S. (1996) Earliest part of Earth's stratigraphic record. *Geology* 24, 43–46.

Rosing, M.T. (1999) 13C-depleted carbon microparticles in> 3700-Ma sea-floor sedimentary rocks from West Greenland. *Science* 283, 674–676.

Russell, W.A., Papanastassiou, D.A., Tombrello, T.A. (1978) Ca isotope fractionation on the Earth and other solar system materials. *Geochimica et Cosmochimica Acta* 42, 1075–1090.

Smithies, R.H. (2000) The Archaean tonalite–trondhjemite–granodiorite (TTG) series is not an analogue of Cenozoic adakite. *Earth and Planetary Science Letters* 182, 115–125.

Szilas, K., Kelemen, P.B., Rosing, M.T. (2015) The petrogenesis of ultramafic rocks in the> 3.7 Ga Isua supracrustal belt, southern West Greenland. *Gondwana Research* 28, 565–580.

Tatsumi, Y. (1989) Boninites and high-Mg andesites: tectonics and petrogenesis. In: Crawford A.J. (Ed.) *Boninites and related rocks*. Unwin Hypman, London, 50–71.

Tusch, J., Sprung, P., van de Löcht, J., Hoffmann, J.E., Boyd, A.J., Rosing, M.T., Münker, C. (2019) Uniform 182W isotope compositions in Eoarchean rocks from the Isua region, SW Greenland. *Geochimica et Cosmochimica Acta* 257, 284-310.

van de Löcht, J., Hoffmann, J.E., Li, C., Wang, Z., Becker, H., Rosing, M.T., Kleinschrodt, R., Münker, C. (2018) Earth's oldest mantle peridotites show entire record of late accretion. *Geology* 46, 199–202.

van de Löcht, J., Hoffmann, J.E., Rosing, M.T., Sprung, P., Münker, C. (2020) Preservation of Eoarchean mantle processes in ~3.8 Ga peridotite enclaves in the Itsaq Gneiss Complex, southern West Greenland. *Geochimica et Cosmochimica Acta* 280, 1-25.

van der Laan, S.R., Flower, M.F.J., Koster Van Groos, A.F. (1989) Experimental evidence for the origin of boninites: Near-liquidus phase relations to 7.5 kbar. In: Crawford A.J. (Ed.) *Boninites and related rocks*. Unwin Hyman, London, 112-147.

Völkening, J., Köppe, M., Heumann, K.G. (1991) Tungsten isotope ratio determinations by negative thermal ionization mass spectrometry. *International Journal of Mass Spectrometry and Ion Processes* 107, 361–368.

Willbold, M., Elliott, T., Moorbath, S. (2011) The tungsten isotopic composition of the Earth's mantle before the terminal bombardment. *Nature* 477, 195.

Wombacher, F., Rehkämper, M. (2003) Investigation of the mass discrimination of multiple collector ICP-MS using neodymium isotopes and the generalised power law. *Journal of analytical atomic spectrometry* 18, 1371–1375.

Young, E.D., Galy, A., Nagahara, H. (2002) Kinetic and equilibrium mass-dependent isotope fractionation laws in nature and their geochemical and cosmochemical significance. *Geochimica et Cosmochimica Acta* 66, 1095–1104.